Computer Life (CPL) ISSN: 1819-4818
DELIVERING QUALITY SCIENCE TO THE WORLD

Residual Reconstruction for Three Dimensional Compressed Sampling of Hyperspectral Images

Li Wang, Wei Wang, Boni Liu

Department of Electronic Engineering, Xi'an Aeronautical University, Xi'an Shaanxi 710077, China

---

Abstract: A residual reconstruction algorithm for Hyperspectral images is proposed to improve the performance of reconstruct algorithm. Firmly believed that the residual arising from spectral prediction and original data is much sparser than the original data, the proposed technique introduced a residual reconstruction method to take advantage of spectral correlation between hyperspectral image bands. Hyperspectral images are divided into groups, and one group consists of a key band followed by some non-key bands. The key and non-key bands are sampled and reconstructed by different methods. The sampling method using three-dimensional compressed sampling (3DCS) could also lift the quality of the reconstructed image. The experimental results reveal that the proposed technique achieves significantly higher quality than a straightforward reconstruction that reconstructs the hyperspectral images band by band independently. The comparison between our sampling method and existing sampling method (block-based compressed sampling) is developed and the results demonstrate that the superiority of our method over other compressed techniques is in terms of high peak signal-to-noise ratio (PSNR) with respect to sampling rate.

Keywords: Hyperspectral images, compressed sampling, residual reconstruction, peak signal-to-noise ratio.

---

1. INTRODUCTION

Hyperspectral images (HSIs) contain rich spatial geometric information and spectral feature information, which is very suitable for target detection, recognition, classification and other fields [1]-[3]. The development of hyperspectral imaging spectrometer [4], the analysis and processing of hyperspectral image data and the research of image interpretation [5]-[7], have become the focus of hot research fields. The continuous expansion of application fields requires hyperspectral images to provide more detailed target information, that is, to improve the spatial resolution and spectral resolution of imaging systems in order to obtain more complete spatial and inter-spectral information. With the sharp increase in people's demand for information, finding effective data compression and reconstruction algorithms is very important for the development of hyperspectral remote sensing technology.

Compressed Sensing (CS) theory was proposed in 2006. It combines sampling and compression processes to directly collect the information characteristics of the data, eliminating the original high-

speed sampling process, and reconstructing the original signal with high accuracy at the reconstruction end. The theory requires that the signal be sparse, capable of random sampling at a sampling rate much lower than the Nyquist sampling frequency, and reconstructing the original signal by an optimized algorithm. Hyperspectral images have redundancy in the spatial and inter-spectral information, and the images are compressible [8]. Compressed sampling and reconstruction of hyperspectral images using compressed sensing theory can greatly reduce the amount of data. The design goal of the reconstruction algorithm is to efficiently and accurately reconstruct the original signal from a small number of measured values. The performance of the algorithm not only determines the quality of the signal reconstruction, but also its computational complexity determines whether it can meet the needs of real-time processing.

Hyperspectral image reconstruction algorithms mainly include: 1) Reconstruction of hyperspectral images using the sparse and smooth characteristics of two-dimensional images, such as the distributed compressed sensing proposed by Liu [9], Fowler's hyperspectral image compression algorithm using principal component analysis [10], and Xu's reconstruction algorithm using Mahalanobis distance tensor [11] as regular terms. 2) Use hyperspectral spatial and inter-spectral features to jointly reconstruct, such as independent sampling and reconstruction of spatial spectrum proposed by August [12], hyperspectral spatial spectrum coding compression proposed by Lin [13], and hyperspectral image reconstruction algorithms based on the idea of blind source separation [14]. 3) Realize using spectral mixing characteristics, estimate end-element features and abundance information to realize reconstruction, such as the the end-element extraction method of spatial combination model proposed by Zhou [15] , Abundance estimation algorithm under sparse, low rank constraints proposed by Giampouras [16], and spatial spectrum reconstruction algorithm [17] proposed by Wang for estimating end elements and abundance information. The amount of hyperspectral image data is large, how to improve the reconstruct algorithm and reduce the computational burden is the focus. In this paper, we are dedicated to improve the performance of reconstruct algorithm via taking advantage of spectral correlation between adjacent bands of HSI.

This paper is organized as follows. The simple measurement method and recovery problem are described and our sampling method (3DCS) is introduced briefly in Section 2. Section 3 develops our proposed reconstruction method, the framework of the proposed method is given and the steps of residual reconstruction are listed with introducing spectral prediction. The experimental results are given in Section 4 to test the performance of the reconstruct algorithm and section 5 gives the concluding remarks.

2. PROPOSED ALGORITHM

The core idea of compressed sensing is that if a signal or image of interest is sparse or compressible in some domain, then it can be reconstructed accurately from very few (relative to the dimension of the signal or image) non-adaptive measurements. Suppose that we want to recover real-valued signal x with length N from M samples such that $M << N$. In other words, we want to recover x from:

$$y = \Phi x \tag{1}$$

Where, y is the measurement value, its length is M, and Φ is an $M \times N$ measurement matrix with sampling rate, being $S = M/N$. We can recover sparse x from the limited number of measurements by a minimum l_0 norm optimization problem,

$$\hat{x} = \arg\min \|x\|_0 \qquad subject\ to \quad y = \Phi x \tag{2}$$

Instead of Gaussian matrix, we introduce the circulant sampling (CirS) to replace a random sampling ensemble with the advantages of easy hardware implementation, memory efficiency and fast decoding. It has been shown that CirS is competitive with random sampling in terms of recovery accuracy. In our previous work, we developed the three dimensional compressed sampling (3DCS) [18] method, consisting of a random permutation, a simple circulant convolution and a random subsampling process, all of which can be performed with little computation or memory. In this paper, we explore the spectral correlation between adjacent bands to improve the quality of reconstructed image.

2.1 Framework of the proposed method

The architecture of our proposed method is depicted in Figure 1. In the framework, hyperspectral images are divided into GOBs (group of bands), and a GOB consists of a key band followed by some non-key bands. $x_{k,key}$ and $x_{k+1,key}$ are the k-th and k+1-th key bands, their corresponding reconstructed bands are $\hat{x}_{k,key}$ and $\hat{x}_{k+1,key}$. $x_{k,i}$ is one of the non-key bands in the k-th group and its reconstructed result is $\hat{x}_{k,i}$. For the key bands, they are measured by 3DCS and reconstructed by the three dimensional total variation (3DTV) method [18]. Turn to non-key bands, we firstly using bi-direction prediction method to obtain predict values from their neighboring reconstructed key bands. Then the residual is calculated from the measurement of original data and the predicted value. The last step is obtaining the reconstructed residual result through 3DTV and revising the predicted value to approach the original data. Our proposed method is denoted as 3DCS-SP.

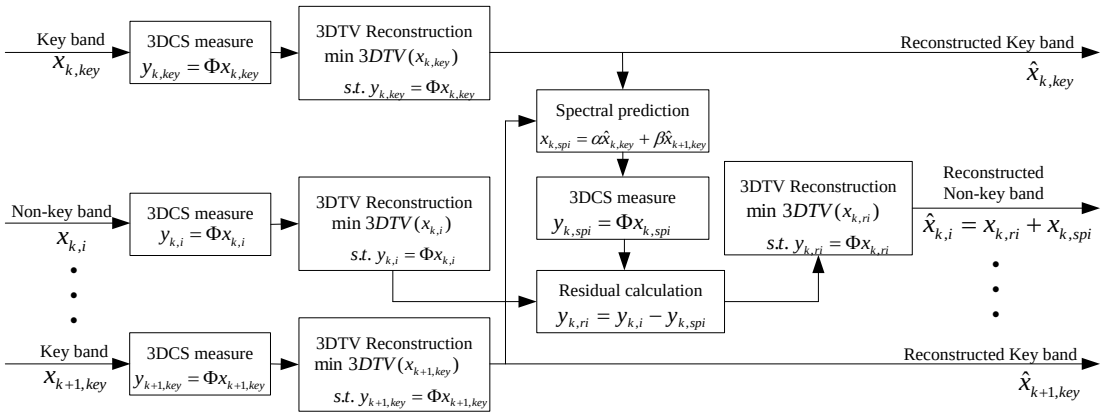

Fig 1. Architecture of our proposed method 3DCS-SP.

2.2 Bi-direction spectral prediction

Hyperspectral images represent the intensities of energy reflected or emitted by the same ground targets with possible hundreds of continuous spectral bands. As a result, there are strong spectral correlations between bands and one band can be fully or partially predicted from other bands. In this paper, the bi-direction interband prediction method is applied to exploit the strong spectral correlation and depicted as follows:

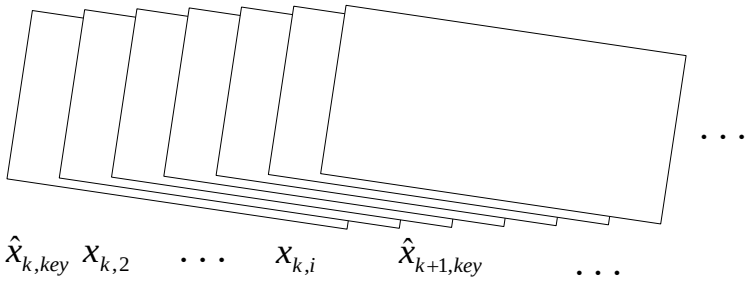

Fig 2. Architecture of bi-direction spectral prediction.

In Figure 2, $\hat{x}_{k,key}$ and $\hat{x}_{k+1,key}$ are reconstructed key bands of k-th and k+1-th group using 3DTV algorithm independently. Assume the distance of $\hat{x}_{k,key}$ and $\hat{x}_{k+1,key}$ is D, which means that the size of group is D, $x_{k,i}$ is a non-key band and the distance between $x_{k,i}$ and $x_{k,key}$ is d, then the prediction of $x_{k,i}$ can be derived from the following equation:

$$x_{k,spi} = \hat{x}_{k,key} + (\hat{x}_{k+1,key} - \hat{x}_{k,key})\frac{d}{D} = \alpha\hat{x}_{k,key} + \beta\hat{x}_{k+1,key}. \tag{3}$$

Where, α and β are defined as:

$$\alpha = \frac{D-d}{D},\ \beta = \frac{d}{D}. \tag{4}$$

2.3 Reconstruction procedure

In our recovery algorithm, 3DTV is used to be the regularization term and the linearly constrained problem can be solved by augmented Lagrangian multipliers (ALM) [19]. In this section, we will describe the residual reconstruction using one non-key band as an example. It contains six steps, namely, key band reconstruction, bi-direction spectral prediction, 3DCS measure, residual calculation, residual reconstruction and non-key band reconstruction.

(1) Key band reconstruction: Use 3DTV to reconstruct $\hat{x}_{k,key}$ and $\hat{x}_{k+1,key}$ independently.

$$\min 3DTV\left(x_{k,key}\right) \quad s.t.\ \ y_{k,key} = \Phi x_{k,key}. \tag{5}$$

$$\min 3DTV\left(x_{k+1,key}\right) \quad s.t.\ \ y_{k+1,key} = \Phi x_{k+1,key}. \tag{6}$$

(2) Bi-direction Spectral prediction: The spectral prediction $x_{k,spi}$ of $x_{k,i}$ is obtained using equation (3).

(3) 3DCS measure: The sampled data of $x_{k,i}$ and $x_{k,spi}$ are described as:

$$y_{k,i} = \Phi x_{k,i}. \tag{7}$$

$$y_{k,spi} = \Phi x_{k,spi}. \tag{8}$$

(4) Residual calculation: Calculate the residual between the measure of original data and the prediction:

$$y_{k,ri} = y_{k,i} - y_{k,spi}. \tag{9}$$

(5) Residual reconstruction: It is clear that $y_{k,ri}$ is the random projection of the residual $x_{k,ri}$, between the original bands and the spectral prediction; i.e.,

$$y_{k,ri} = y_{k,i} - \Phi x_{k,spi} = \Phi\left(x_{k,i} - x_{k,spi}\right) = \Phi x_{k,ri}. \tag{10}$$

The recovery problem is written as:

$$\min 3DTV\left(x_{k,ri}\right) \quad s.t. \;\; y_{k,ri} = \Phi x_{k,ri} \tag{11}$$

(6) Non-key band reconstruction: Let $\hat{x}_{k,ri}$ be the recovery from $y_{k,ri}$; consequently, we can obtain an approximation reconstruction to $x_{k,j}$ as:

$$\hat{x}_{k,i} = \hat{x}_{k,ri} + x_{k,spi}. \tag{12}$$

It should be noted that the measurement matrix above are the same which means that the sampling rate for the key bands and non-key bands are same. In fact, in the following experiments, we will study whether the sampling rate of key bands and non-key bands will influence the reconstruct result. We will focus our attention on four cases: (1) 2DCS: All bands are sampled with the same sampling rate and the sampling method is 2DCS (not considering the spectral correlation between the adjacent bands). (2) 3DCS: All bands are sampled with the same sampling rate and the sampling method is 3DCS. (3) 3DCS-SP-same: The suffix 'same' means that the key bands and non-key bands are sampled with the same sampling rate and using residual reconstruction for the non-key bands. (4) 3DCS-SP-diff: Here the 'diff' means the key bands are sampled at a relatively high sampling rate, while the non-key bands are at an identical lower sampling rate.

3. EXPEMENTAL RESULTS

We now examine the performance of residual reconstruction on hyperspectral data. Two hyperspectral data cube are used in the experiment. The first cube is the scene of city Changzhou supported by Shanghai Institute of Technical Physics, Chinese Academy of Sciences and the office 308 of National 863 program. The second cube is the cuprite scene from AVIRIS (http:// aviris.jpl.nasa.gov). We choose first 64 bands and intercept a sub-region to simulate, so the simulation data has 64 bands and the image size is 256*256. In the following paper, the first type data is denoted as scene1, while the second type is scene2. And a GOB size is 8.

As a primary measure of reconstruction quality, we calculate the peak signal-to-noise (PSNR) of the reconstructed image to evaluate the performance of different reconstruction algorithms. For 3DCS-SP, various sampling rates are employed for the key bands as well as the non-key bands; thus, we have two sampling rates in use: the key bands sampling rate S_{key}, and the non-key bands sampling rate $S_{non-key}$. First, we consider the case wherein all bands are sampled at the same sampling rate, i.e., "equal" sampling with $S_{key} = S_{non-key}$. Then, we consider the case wherein the key bands have an increased sampling rate with respect to the non-key bands, i.e., $S_{key} > S_{non-key}$. In these two situations, PSNR results are averaged over only the non-key bands. A summary of the results from the four methods is presented in Table 1.

Table 1. Average PSNR in dB for scene1 and scene2

S_{key}	2DCS	3DCS	3DCS-SP-same $S_{key} = S_{non-key}$	3DCS-SP-diff $S_{key} > S_{non-key}$

Scene1				
0.1	24.8286	27.3570	30.6060	33.3398
0.2	25.9862	29.9534	34.4562	36.1930
0.3	27.4717	32.7602	37.5218	38.5438
0.4	29.0886	34.4642	39.5542	40.3028
0.5	30.7660	36.2892	41.7059	42.1305
Scene2				
0.1	27.4299	32.8656	38.3287	42.2025
0.2	29.9530	36.3948	42.2967	44.0664
0.3	32.0796	39.5557	44.3437	44.9072
0.4	33.8587	41.2981	45.1479	45.3674
0.5	35.4185	42.7288	45.5561	45.5965

Since the key bands constitute only a small number of the total bands in hyperspectral images, and they serve somewhat as "anchors" to the spectral prediction process of reconstruction in a GOB, it is reasonable to consider the situation in which key bands are given a higher sampling rate than the non-key bands such that they are reconstructed with higher quality. Thus, we perform a battery of experiments which measure the PSNR when the sampling rate for key bands is increased beyond that of the non-key bands. Figure 3 depicts the performance of 3DCS-SP-diff when $S_{key} = 0.8$ while $S_{non-key}$ varies between 0.1 and 0.5. PSNR is averaged over all non-key bands of two hyperspectral data. 3DCS-SP-same refers to the sampling rate of key bands and non-key bands are the same, while 3DCS-SP-diff means the sampling rate are different. The sampling rate in the experiment are $S_{key} = 0.8$ and $S_{non-key}$ varies between 0.1 and 0.5. In these graphs, we also compare the 3DCS-SP results with 3DCS without residual reconstruction. As expected, the residual reconstruction method with prediction from reconstruction of the key bands results in a significant performance improvement for 3DCS-SP-diff. From the right of Figure 3, we can discover that our method shows a great advantage especially at a lower sampling rate. The PSNR of method 3DCS-SP-diff is up to 9dB higher than 3DCS without residual reconstruction.

We now compare the performance of 3DCS-SP to that of the technique of [20]. In this technique, the image is partitioned into smaller blocks. The sampling of the image is driven by random matrices applied on a block-by-block basis, while the reconstruction is a variant of projected Landweber reconstruction that incorporates a smoothing operation intended to reducing blocking artifacts. And in this paper, in order to compare our sampling method with this BCS method, we also use the spectral prediction in the reconstruction process, so the method is denoted as BCS-SP. Here, we compute the PSNR to evaluate the performance of the sampling method. The result of this experiment is shown in Figure 4 (the suffix 'same' and 'diff' has the same meaning as before). The sampling rate of the key bands and non-key bands are same in the left of Figure 4, we can see that our method has the highest PSNR among the three methods, and the technique BCS is the lowest. The result also depicts that our

sampling method 3DCS without spectral prediction in the reconstruction process can also achieve higher PSNR than the sampling method BCS with residual reconstruction. In the right of the figure, at the lower sampling rate, the method BCS-SP will give a better result than 3DCS, whereas, the situation has changed a little bit with the sampling rate increasing. But, we can still conclude that our proposed residual reconstruction plus sampling method 3DCS can give the best reconstruct results whatever the sampling rate is.

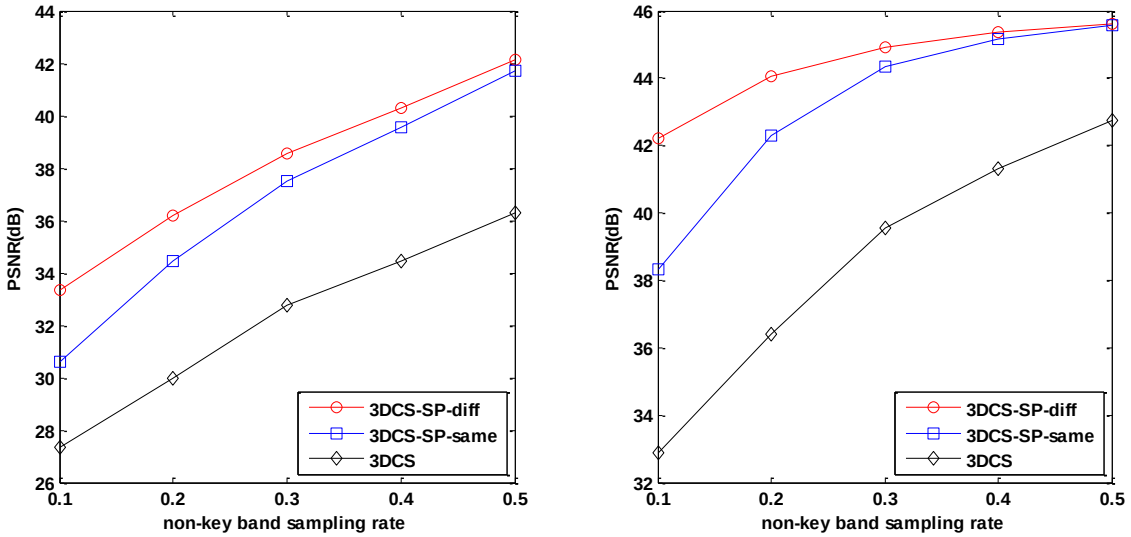

(a) Scene1 (b) Scene2

Fig 3. Performance of method 3DCS-SP at different situation.

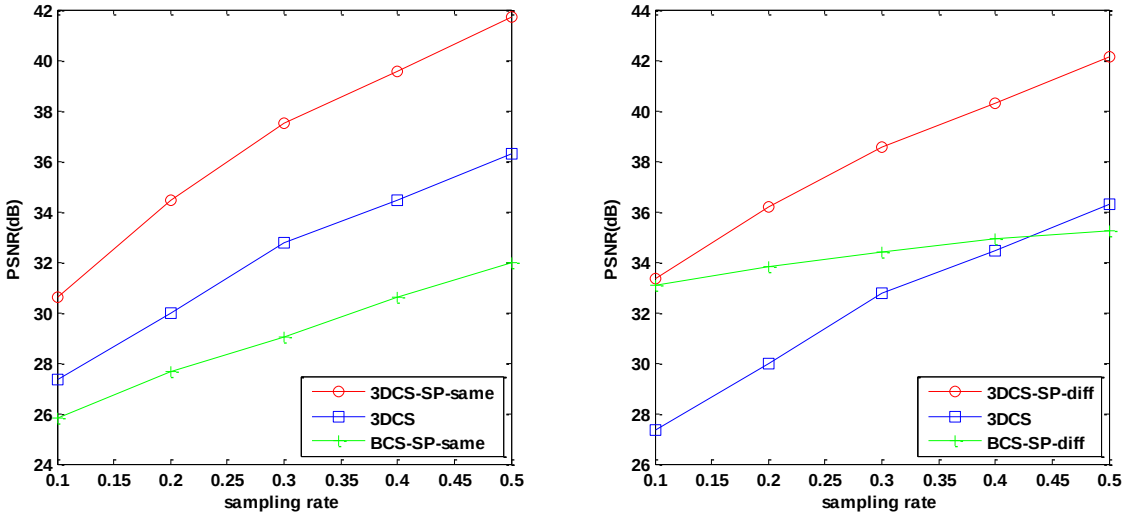

(a) same (b) different

Fig 4. Comparison to the technique due to James E.Fowler.

4. CONCLUSION

In this paper, we focused on reconstruction driven by 3D circulant convolution sampling process, employing the spectral prediction to improve the reconstruction quality. While independent reconstruction is fast and straightforward, improved reconstruction quality resulted from exploiting

the spectral prediction and the different sampling rate of the key bands and non-key bands is very effectively especially in the reconstruct of hyperspectral images. Incorporating reconstruction from a spectral prediction based residual, the 3DCS-SP technique we proposed here alternatively reconstructs residual arise from the spectral prediction and the original data to improve the quality of the non-key bands.

Extensive experiment results demonstrate that our proposed residual reconstruction can obtain higher PSNR over 3DCS that does not utilize the correlation of the adjacent bands in the reconstruct process. In order to study how the sampling rate of key bands and non-key bands influence the reconstruct results, we have compared the results of our method 3DCS-SP-same and 3DCS-SP-diff. For different hyperspectral images, when the sampling rate of key bands is larger than the non-key bands (denoted as 3DCS-SP-diff), the method will get better reconstruct result especially the sampling rate of the non-key bands is at a lower level. In addition to this, we compare our proposed method 3DCS-SP and the existing sampling method BCS which use our residual reconstruction algorithm in the reconstruct process. We also consider the different sampling rate for key or non-key bands, and the results consistently show that our sampling method 3DCS incorporating our residual reconstruction is very efficient in the compressive of hyperspectral images whatever the sampling rate is.

ACKNOWLEDGMENTS

This work was supported by the National Natural Science Foundation of China (grant number 61901350); Scientific Research Plan Projects of Shaanxi Education Department (grant number 19JK0432) and Science Research Fund of Xi'an Aeronautics University (grant number 2019KY0208).

REFERENCES

[1] CAI Q, LI E, JIANG J, et al. Study on the Tea Identification of Near-Infrared Hyperspectral Image Combining Spectra-Spatial Information [J]. Spectroscopy and Spectral Analysis, 2019, 39(08): 2522-2527.

[2] NIU Y and WANG B. Extracting Target Spectrum for Hyperspectral Target Detection: An Adaptive Weighted Learning Method Using a Self-Completed Background Dictionary [J]. IEEE Transactions on Geoscience and Remote Sensing, 2017, 55(3): 1604-1617.

[3] CHEN S, ZHOU Y, QI R. Joint Sparse Representation of Hyperspectral Image Classification based on Kernel Function [J]. Systems Engineering and Electronics, 2018, 40(3): 692-698.

[4] CHANG C I. A Review of Virtual Dimensionality for Hyperspectral Imagery [J]. IEEE Journal of Selected Topics in Applied Earth Observations and Remote Sensing, 2018, 11(4): 1285-1305.

[5] ALSUWAIDI A, GRIEVE B and YIN H. Feature-Ensemble-Based Novelty Detection for Analyzing Plant Hyperspectral Datasets [J]. IEEE Journal of Selected Topics in Applied Earth Observations and Remote Sensing, 2018, 11(4): 1041-1055.

[6] TANG Z， FU G, CHEN J, et al. Low-rank Structure Based Hyperspectral Compression Representation [J]. Journal of Electronics & Information Technology, 2016, 38(05): 1085-1091.

[7] HAUNG D, ZHANG X, ZHANG M, et al. Feature Extraction of Hyperspectral Images Based on Semi-Supervised Locality Preserving Projection with Spatial-Correlation [J]. Laser & Optoelectronics Progress, 2019, 56(02): 021003.

[8] YIN J, SUN J, and JIA X. Sparse Analysis Based on Generalized Gaussian Model for Spectrum Recovery with Compressed Sensing Theory [J]. IEEE Journal of Selected Topics in Applied Earth Observations and Remote Sensing, 2015, 8(6): 2752-2759. DOI: 10.1109/JSTARS.2014.2336834.

[9] Liu H, Li Y, Xiao S, et al. Distributed Compressive Hyperspectral Image Sensing [C]. IEEE Sixth

International Conference on Intelligent Information Hiding and Multimedia Signal Processing, Darmstadt, DE, Oct. 15-17, 2010: 607-610.

[10] James E.Fowler, Sungkwang Mun, and Eric W. Tramel. "Multiscale block compressed sensing with smoothed projected Landweber reconstruction". Proceedings of the European Signal Processing Conference, Barcelona, Spain, August 2011.

[11] Xu Y, Wu Z, Chanussot J, et al. Joint Reconstruction and Anomaly Detection from Compressive Hyperspectral Images Using Mahalanobis Distance-Regularized Tensor RPCA [J]. IEEE Transactions on Geoscience and Remote Sensing, 2018, 56(5): 2919-2930.

[12] August Y, Vachman C, Rivenson Y, et al. Compressive Hyperspectral Imaging by Random Separable Projections in both the Spatial and the Spectral Domains [J]. Applied Optics, 2013, 52(10): 46-54.

[13] Lin X, Liu Y B, Wu J M, et al. Spatial-Spectral Encoded Compressive Hyperspectral Imaging [J]. ACM Transactions on Graphics, 2014, 33(6): 1-11.

[14] Golbabaee M, Arberet S and Vandergheynst P. Compressive Source Separation: Theory and Methods for Hyperspectral Imaging [J]. IEEE Transactions on Image Processing, 2013, 22(12): 5096-5110.

[15] Zhou Y, Rangarajan A and Gader P D. A Spatial Compositional Model for Linear Unmixing and Endmember Uncertainty Estimation [J]. IEEE Transactions on Image Processing, 2016, 25(12): 5987-6002.

[16] Giampouras P V, Themelis K E, Rontogiannis A A, et al. Simultaneously Sparse and Low-Rank Abundance Matrix Estimation for Hyperspectral Image Unmixing [J]. IEEE Transactions on Geoscience and Remote Sensing, 2016, 54(8): 4775-4789.

[17] Wang Z, Feng Y and Jia Y. Spatio-Spectral Hybrid Compressive Sensing of Hyperspectral Imagery [J]. Remote Sensing Letters, 2015, 6(3): 199-208.

[18] Li Wang, Yan Feng. "Hyperspectral Imaging via Three-dimensional Compressed Sampling", International Conference on Advanced Computer Science and Electronics Information (ICACSEI 2013), 355-359,Beijing, China, July 2013.

[19] J Yang, Y Zhang, and W Yin. "A Fast Alternating Direction Method for TVL1-L2 Signal Reconstruction From Partial Fourier Data". IEEE journal of selected topics in signal processing, 4(2), (2010).

[20] Fowler J E and Du Q. Reconstructions from Compressive Random Projections of Hyperspectral Imagery [M]. In Optical Remote Sensing: Advances in Signal Processing and Exploitation Techniques, edited by Prasad S., Bruce L. M., and Chanussot J, Berlin: Springer Berlin Heidelberg, 2013: 31-48.